DOI: 10.31401/WS.2025.proc.08

Application of Microwave Average Time Profile to Analysis of Flares with Long-Duration Energy Release

Motyk I.D., Kashapova L.K., Rozhkova, D.V.

Institute of solar-terrestrial physics, Siberian Branch of Russian Aacademy of Sciences
motykilya@iszf.irk.ru

Abstract

We present results of study of a powerful solar flare using microwave average temporal profiles describing elementary processes of electron acceleration and precipitation. The average profile was reconstructed using simple single-peak profiles of solar flares observed in a wide range of frequencies (3-24 GHz) using the Siberian Radioheliograph. Analysis of these profiles confirms the dominance of non-thermal emission in their formation. The template for analysis includes both the average profile and an analytical approximation, which combines a fourth-order polynomial for the rising phase and two exponential functions for the decaying phase. Applying our method to the microwave temporal profile of the X1.8 long-duration flare on October 9, 2024, we revealed three secondary energy release events that occurred after the main impulsive phase and estimated their characteristics. Analysis of event characteristics reveals a gradual increase in event power - the first two events were not distinguishable in hard X-ray profiles due to low electron fluxes. The results demonstrate the effectiveness of microwave average temporal profiles in detecting secondary energy release, and their usefulness for studying long-duration flares.

Keywords: Solar flares; average time profile; microwave emission;

1. Introduction

The most of current solar flare models describe scenarios of “simple” or “classical” solar flares where the key element is single main act of energy release. However, many flares are more complex and cannot be described by these models. For example, long-duration events are not explained by these models and require a different approach. In these flares, the observed time for flare emission decay is longer than 2 hours, and explaining by plasma cooling only does not satisfy qualitative estimations based on theoretical predictions. Nowadays it can be explained by additional processes that occur during flare, such asadditional acts of energy release, which we are focused on. However, the role of these processes and their contribution to extending the flare cooling time is unclear. We can better understand this by presenting a complex flare as a set of multiple simple events that can be studied and evaluated separately. In order to separate the main flare from other events that follow it, we need to understand the general behavior of a "classical" flare and describe it using a template or an average time profile. Then, this average time profile can be applied to the flare and help us to reveal the parameters of each event of energy release. The method showed its usefulness in analysing white-light flares on M4 red-dwarf star in [Davenport et al., 2014]. The average time profiles were constructed for UV/EUV [Kashapova et al., 2021] and soft X-ray [Gryciuk et al. 2017] emission of solar flares. In this paper, we focus on an average microwave time profile, because the microwave emission provides useful information about the emission mechanism and parameters of flare plasma for both powerful and weak events. The aim of this paper is to show the application of an average microwave profile for analyzing events.

2. Data and processing techniques

The average temporal profile (hereinafter, the average profile) is a temporal profile, derived from a set of flares with simple shape of temporal profiles. We define the average profile as the temporal profile of a flare, which follows a classic scenario describing only one increase in flux and a slow decay.

As mentioned above, the microwave (MV) emission from solar flares is a sensitive indicator of the electron fluxes and their properties, as well as the mechanisms that generate this emission. Therefore, an analysis of the spectrum shape can reveal thermal or non-thermal mechanisms of emission generation. As it is better to create an average profile of emission from the same mechanism, there is a need for a wide range of observations with high spectral resolution in order to select flares with the shape of the spectrum typical for gyrosynchrotron emission of non-thermal electrons. The Siberian Radioheliograph (SRH) [Altyncev et al., 2020] provides data well suitable for these purposes. It is a radio interferometer operating on 48 frequencies within the 3–24 GHz range with high temporal resolution (~ 3.5 s.) and high flux sensitivity (~0.001 sfu). Except for radio images it also provides “sun-as-a-star” flux observations with high flux sensitivity.

For average profile reconstruction we used events selected by automatic event detection algorithm [Rozhkova et al., 2024]. Preliminary it was found ~600 candidates during the period of July–September 2023 and May 2024. We select events with simple temporal profiles from the candidates, applying the following criteria of a "classical" profile: there is only one emission maximum, a fast rise phase and a gradual decay phase. Fluctuations in the emission in a temporal profile must not exceed 30% of the maximum value.

As a result, we selected 116 dynamic spectra of the flares with “classical” temporal profiles and the shape of microwave spectrum that is characteristic of gyrosyncrotron emission of non-thermal electrons. The microwave spectrum of the flare consists of optically thin and thick emission sources which are formed in different regions of flare loop (footpoints and top). So, we have to separate the emission coming from them. One of the ways to separate them is using peak frequency of the spectrum [Dulk, 1985]. The emission at frequencies below the peak frequency are from optically thick emission source and the emission above peak frequency is from optically thin source.

Each time profile has different intensity and duration, and in order to reveal the general behaviour of both powerful and weak events we need normalize them by both intensity and time. We normalized the intensity (or flux) at each frequency and then scaled the time to the half-width of the time profile ($t_{1/2}$) at a half-intensity as it was done in [Davenport et al., 2014]. Then, we derived normalized temporal profiles for optically thick and optically thin sources for each event. At the final step of average profile construction, we interpolated all profiles onto a grid with 0.001 $t_{1/2}$ time bins. The median values in each time bin formed the average profiles presented in fig. 1. As can be seen, the average profiles of emission from both optically thin and thick sources are very similar. The correlation coefficient between these profiles is 0.99, which means that they are identical. Usually, differences between the temporal profiles originating at different levels of a flare loop occur in cases of process related with thermal plasma. One example is filling the top by hot plasma or chromospheric evaporation. Similarity indicates that the average profiles show the process of accelerated electron precipitation during a solar flare.

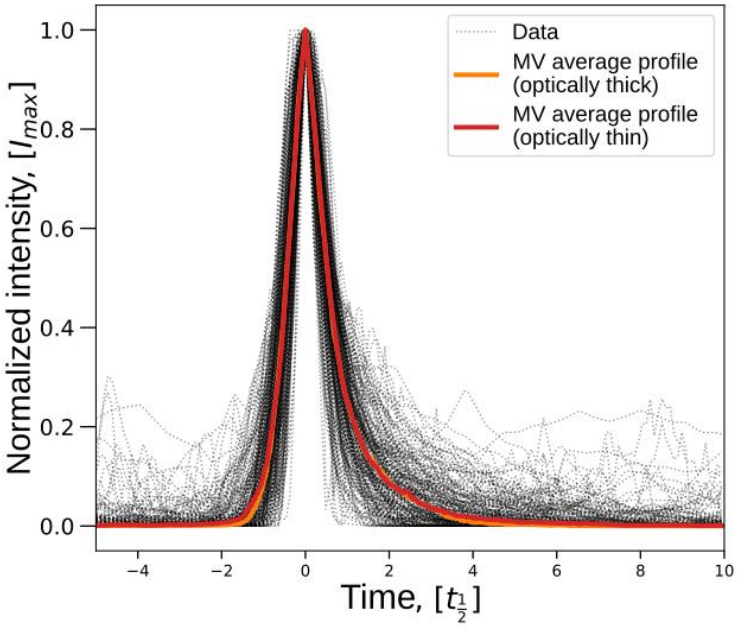

Figure 1. *Average time profiles of microwave emission of a solar flare for emission of different part of a flare loop.*

Based on constructed average profiles, we obtained analytical approximations, which consist of 4-order polynomial function for rise phase and two exponential functions for the decay phase. The found coefficients of the mentioned functions are presented in [Motyk et al., 2025]. By using analytical approximations, we developed a method that allows us to analyze flares for presence of accelerated electrons. We tested this method on the C1.2 class flare took place on Feburary 3, 2022. The analysis revealed two events of accelerated electron participation. One was due to a flare, and the other was due to an additional energy release event. Successful identification of weak events in small flare assumes the opportunity that we can apply our method to other more powerful events.

3. Application results and discussion

We applied our approach to the X1.8 flare that occurred on October 9, 2024. Its maximum was at about 01:56 UT. It lasted approximately 7 hours and was a long-duration event. The 1700 Å band images by SDO/AIA [Lemen et al., 2012] (fig. 2) show two ribbons located in the center of the solar disk. One of the ribbons was located within a sunspot, one of which was located in a sunspot. Usually, at first, we observe the maximum hard X-ray or microwave emission, and then the soft X-ray emission corresponds to the increasing density of heated plasma. Thus, the processes of acceleration and heating are going sequentially.

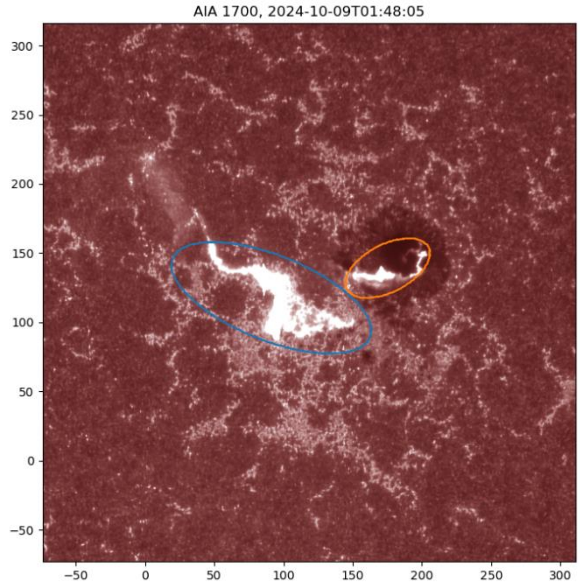

Figure 2. *Active region with highlighted ribbons of X1.8 flare at 01:48 UT which is approximately at the maximum of microwave emission. Blue and orange ovals indicate the regions used to get flux data in order to reconstruct the temporal profiles of ribbons 1 and 2, correspondingly.*

Analysis of the MV spectrum of the flare at its temporal profile maximum (UT 01:47) reveals that the emission mechanism was gyrosynchrotron, and the peak frequency separating the emission from optically thick and optically thin sources was at about 7 GHz. It means that the temporal profiles at frequencies higher than the trace processes of acceleration and precipitation of electrons. Figure 3 (left panel) presents the temporal profiles of 12.2 GHz MV emission and non-thermal X-ray emission in the 50-100 keV band by FERMI/GBM [Meegan et al., 2009]. The application of the average profile (AP) reveals that the flux after the temporal profile maximum at 12.2 GHz is significantly higher than predicted. After subtracting the average profile from the flare profile, three bursts of the decay phase in MV emission became more pronounced. In the subtracted MV time profile. We found three small bursts at 01:48 UT, 01:50 UT, and 01:55 UT that were well described by average profiles (APs). The properties of these APs, such as half-width and flux, are presented in Table 1.

Table 1. *Half-widths $t_{1/2}$ and maximum flux of average profiles (APs) of the flare and bursts on decay phase of microwave emission.*

	Half-width $t_{1/2}$, s	**Maximum flux, sfu**
Flare	137.5	834.31
Burst 1	23.0	133.18
Burst 2	52.5	286.27
Burst 3	121.0	392.80

As can be seen from Fig. 3 and Table 1, the main impulsive peak of the flare was accompanied by two fast and relatively small bursts associated with accelerated electron precipitation (bursts 1 and 2), which were not visible in the temporal profiles of hard X-ray emission. The last burst can be seen in both MV and hard X-ray temporal profiles. It has almost the same half-width as the main impulse burst, and the flare was more powerful than the previous two bursts. The reason why the first two bursts are not visible in hard X-rays may be due to the higher sensitivity of MV emission to electron fluxes. Therefore, we see a gradual increase in the power of non-thermal energy release after the main impulsive phase. We note that this process occurred simultaneously with the passing of the maximum temperature and reaching of the emission measure maximum.

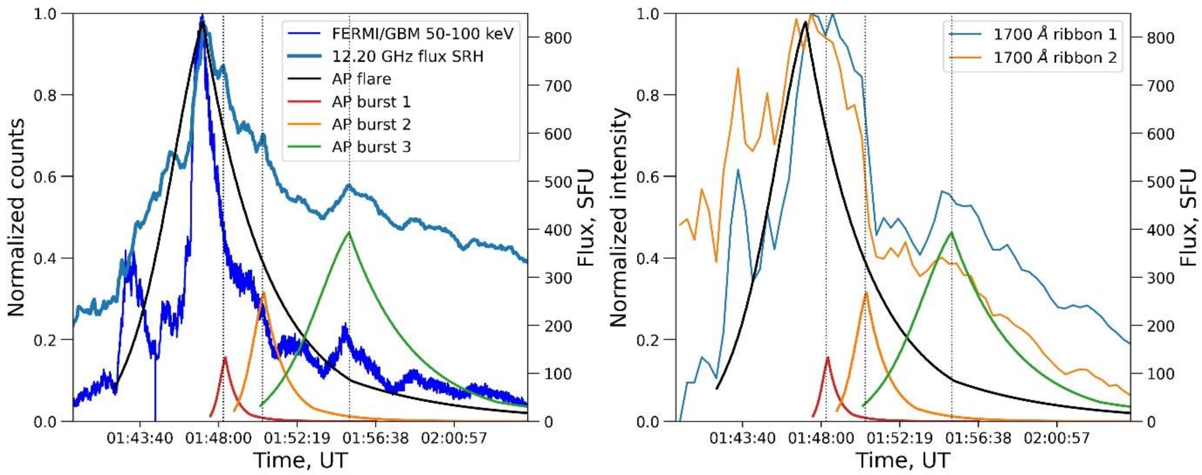

Figure 3. *Left panel: Microwave, hard X-ray temporal profiles and templates of flare and three bursts. The vertical lines show time of the maximum of each burst template. Right panel: Comparison of the evolution of emission flare ribbons at 1700 Å in the SDO/AIA band and templates of flares and three bursts. The temporal profiles of flare ribbon 1 and 2 are shown by the same color as they are marked on fig 2.*

The temporal profiles taken from the flare ribbon regions using 1700 Å AIA/SDO band images are presented in the left panel of Figure 3. The profile of ribbon 1 shows the evolution of the left ribbon intensity (see Fig. 2). The profile of ribbon 2 presents the intensity of the right flare ribbon located in the sunspot area. As one can see, that despite of low temporal resolution of the data (24 seconds), the flux of the temporal profile of ribbon 2 precedes the bursts seen in the profile of ribbon 1 during the impulse phase. This behavior changed after 1:50 UT, when the heating process began to dominate. This may be explained by the fact that ribbon 2 is closely associated with the site of initial energy release during the impulse phase. It is possible that the location of the energy release moved, and we began to detect a first response to these events through the emission of ribbon 1.

We note that the revealed MW bursts 1 and 2 precede the bursts seen in the temporal profiles of the 1700 Å band, while the hard X-ray profile did not show pronounced bursts at that moment. As can be seen, the temporal profile of region 1 has a small but pronounced peak around the same time as MW burst 3 (AP3). On the other hand, the temporal profile of ribbon 2 continues to decrease gradually. The difference in behaviour between the profiles indicates that the location of the burst 3 is closely related to the ribbon 1.

4. Conclusions

We applied the reconstructed microwave average temporal profile of a "classical" solar flare to the analysis of a powerful and long-lasting solar flare. The average temporal profile was obtained for gyrosynchrotron emission of non-thermal electrons and traced the process of acceleration and precipitation of electrons. As a comparison of the average temporal profiles formed at different levels of flare loop for the ideal case of gyro-synchrotron emission generation by accelerated electrons revealed that they were identical, we neglected thermal plasma effects in the interpretation of the results. As it was shown in the example of a weak solar flare on February 3, 2022, analysis of temporal profiles can be done by fitting them with a combination of average profiles or analytical functions or templates describing the behavior of the microwave temporal profile. The application of the suggested technique to study the temporal profiles of microwave emission from powerful flares on October 9, 2024 revealed that three additional energy release events occurred between the main impulsive peak in maximum soft X-rays and the flare. The presence of these bursts and their separation by the average profile indicates several events of electron acceleration occurring after the main impulse phase. The two first additional bursts are not seen in hard X-rays, which can be explained by the low sensitivity of this kind of emission to electron fluxes. Analysis of the average profiles obtained for each event allowed getting characteristics such as time duration, half-width at half intensity, and flux level at 12.2 GHz frequency. The dynamics of these parameters show a steep decrease in the power and duration of the acceleration and precipitation processes. Then, the power of the process gradually increases over time towards the last extracted event. There were seen two flare ribbons in the 1700 Å SDO/AIA band images, one of which (ribbon 2) was located in the sunspot area. In addition, we conducted a comparison of the temporal profiles of emissions from flare ribbons observed in the SDO/AIA 1700 Å band and found that the latest revealed burst was more pronounced in the temporal profile of ribbon 1, which is located outside the sunspot. This can be an indicator of the movement of the initial energy release from a sunspot close to another ribbon.

Acknowledgements and funding

The authors thank the teams of the Siberian Radioheliograph (Institute of Solar-Terrestrial Physics SB RAS), GOES, SDO and FERMI for providing open access to observational data. This study was supported by the grant of the Russian Science Foundation No. 24-22-00315, https://rscf.ru/en/project/24-22-00315

References

Altyntsev, A.T., Lesovoi, S.V., Globa, M.V., et al. (2020). Multiwave Siberian Radioheliograph, *Solar–Terrestrial Physics*, Vol. 6, No. 2, pp. 30–40, DOI: 10.12737/stp-62202003.

Davenport, J.R.A., Hawley, S.L., Hebb, L., et al. (2014). Kepler flares. II. The temporal morphology of white-light flares on GJ 1243, *Astrophysical Journal*, Vol. 797, No. 2, pp. 122–133, DOI: 10.1088/0004-637X/797/2/122.

Dulk, G.A. (1985). Radio emission from the Sun and stars, *Annual Review of Astronomy and Astrophysics*, Vol. 23, pp. 169–224, DOI: 10.1146/annurev.aa.23.090185.001125.

Gryciuk, M., Siarkowski, M., Sylwester, J., et al. (2017). Flare characteristics from X-ray light curves, *Solar Physics*, Vol. 292, No. 6, 77, DOI: 10.1007/s11207-017-1101-8.

Kashapova, L.K., Broomhall, A.-M., Larionova, A.I., et al. (2021). The morphology of average solar flare time profiles from observations of the Sun's lower atmosphere, *Monthly Notices of the Royal Astronomical Society*, Vol. 502, No. 3, pp. 3922–3931, DOI: 10.1093/mnras/stab276.

Lemen, J.R., Title, A.M., Akin, D.J., et al. (2012). The Atmospheric Imaging Assembly (AIA) on the Solar Dynamics Observatory (SDO), *Solar Physics*, Vol. 275, No. 1–2, pp. 17–40, DOI: 10.1007/s11207-011-9776-8.

Meegan, C., Lichti, G., Bhat, P.N., et al. (2009). The FERMI gamma-ray burst monitor, *Astrophysical Journal*, Vol. 702, No. 1, pp. 791–804, DOI: 10.1088/0004-637X/702/1/791.

Motyk, I.D., Kashapova, L.K., Rozhkova, D.V. (2025). Average temporal profiles of solar flare microwave emission: Morphology and application, *Astronomy Reports*, Vol. 69, No. 6, pp. 519–531, DOI: 10.1134/S1063772925701860.

Rozhkova, D., Kashapova, L., Gubin, A. (2024). A method to reveal and catalog solar flares observed with the Siberian Radioheliograph: First results, in: *Modern Astronomy: From the Early Universe to Exoplanets and Black Holes (VAK-2024)*, pp. 1129–1133, DOI: 10.26119/VAK2024.181.